Gold Bull (2016) 49:21–33
DOI 10.1007/s13404-016-0179-3

ORIGINAL PAPER

Synthesis of gold nanoparticles under highly oxidizing conditions

Tanja Jurkin[1] · **Martina Guliš**[2] · **Goran Dražić**[3] · **Marijan Gotić**[1]

Received: 26 October 2015 / Accepted: 22 February 2016 / Published online: 8 March 2016

Abstract Gold nanoparticles (AuNPs) were synthesized in a microemulsion water/Triton X-100/1-pentanol/cyclohexane using various reducing agents. Basically, three microemulsion syntheses of AuNPs were studied: (i) one using a strong chemical reducing agent ($NaBH_4$), (ii) another using γ-irradiation under moderately strong reducing/oxidizing conditions, and (iii) yet another under highly oxidizing conditions (with the addition of NaOH aqueous solution). All the three were performed at room temperature. When a strong chemical reducing agent $NaBH_4$ was used in the microemulsion, gold crystallites 11.7 nm in size were obtained, as determined on the basis of X-ray powder diffraction line broadening. The γ-irradiation of nitrogen-saturated microemulsion at the acidic pH produced AuNPs about 12 nm in size, which under the isolation by centrifugation aggregated into large preconcentrated AuNPs about 150 nm in size. These AuNPs possess thixotropic properties. The microemulsion stirred at room temperature and at the pH < 7 under oxidizing conditions did not produce gold nanoparticles. Under the identical experimental conditions and at the pH > 7 (stronger oxidizing conditions), well-dispersed AuNPs 12 nm in size were formed. The microemulsion synthesis of AuNPs in the alkaline range but not at an acidic pH was explained by the oxidation of alcohol groups (–OH) into carbonyl groups (>C=O) due to the catalytic action of hydroxyl ions and gold. In parallel with the catalytic oxidation of alcohol groups in microemulsion, the Au(III) were reduced with the subsequent formation of gold nanoparticles. The synthesis of AuNPs in 1-pentanol by adding the aqueous NaOH solution at room temperature without using microemulsions confirmed the role of the base-catalyzed oxidation of alcohols in the formation of AuNPs. Based on the findings in this study, we propose the base-catalyzed alcohol oxidation at room temperature as a new, simple, and versatile synthesis route for obtaining gold nanoparticles. The results of this study suggest that the classical approach of using a reducing agent for the synthesis of AuNPs is not a determining factor, since a diametrically opposite approach to the synthesis of AuNPs can be used, namely, stimulating the oxidation of the functional organic groups in close proximity to gold ions.

Keywords Gold nanoparticles · Microemulsion · Alcohol · Oxidizing conditions · Base catalyzed · Cloud point extraction

Electronic supplementary material The online version of this article (doi:10.1007/s13404-016-0179-3) contains supplementary material, which is available to authorized users.

✉ Marijan Gotić
gotic@irb.hr

Tanja Jurkin
tjurkin@irb.hr

Martina Guliš
martina.gulis@gmail.com

Goran Dražić
goran.drazic@ki.si

[1] Division of Materials Chemistry, Ruđer Bošković Institute, Bijenička 54, Zagreb, Croatia

[2] Faculty of Chemical Engineering and Technology, University of Zagreb, Marulićev trg 19, 10000 Zagreb, Croatia

[3] Laboratory for Materials Chemistry, National Institute of Chemistry, Hajdrihova 19, SI-1001 Ljubljana, Slovenia

Introduction

Gold nanoparticles (AuNPs) are widely used in analytical chemistry [1, 2], in biomedicine [3, 4], and as catalysts [5–9]. In biomedicine, AuNPs are used as biosensors [10,

11] and as carriers for targeted delivery of drug to specific sites in the body [12, 13], as well as new contrast and radiosensitization agents [14–17]. Gold is a noble (inert) element; however, at the nanoscale, the gold exhibits catalytic activity for the oxidation of alcohols and carbon monoxide [6–9]. In addition to the applications, the synthesis of gold nanoparticles is one of the best model systems for the study of nucleation and crystal growth. During synthesis, many parameters influence the physicochemical properties of the obtained gold nanoparticles [18]. The choice of reducing agent and electrostatic stabilization of AuNPs in aqueous solutions fall into two very important parameters in the synthesis of gold nanoparticles. For instance, in the classical citrate method [19, 20], the citrate ions have a dual role; they are reducing agent and at the same time they stabilize AuNPs against precipitation in the aqueous media. However, the citrate ions are weakly reducing agent that is not able to easily reduce Au(III) ions in aqueous solution at room temperature. The classical citrate synthesis is therefore carried out usually at temperatures above 70 °C. Recently, Hanžić et al. [21] synthesized AuNPs via a citrate method using radiolytical synthesis at room temperature. It was shown that γ-irradiation produced well-dispersed, stable, and highly concentrated AuNPs in an aqueous citrate solution in the presence of dissolved oxygen and without adding any reducing or stabilizing agents. It was emphasized that radiolytically intensified citrate oxidation and decarboxylation to dicarboxyacetone, acetone, and other products were advantageous for Au(III) reduction and subsequent formation of gold nanoparticles. The radiolytical oxidation of citrate groups that were bound to the gold ions enabled the formation of AuNPs in the highly oxidizing environment at room temperature. Thus, the classical approach of using a reducing agent to synthesize AuNPs is not a determining factor, since diametrically different approaches can be used for the synthesis of AuNPs, namely, in stimulating the oxidation of the organic molecules that are bound to gold ions [21].

In this work, the gold nanoparticles were synthesized using microemulsion technique [22–30]. Microemulsions are self-assembling stable dispersion systems consisting of water, oil, and surfactant (surface active agents). The water-in-oil (w/o) microemulsions comprise dispersed water droplets in the oil phase. Ideally, the water droplets (aqueous core) are completely enveloped by protective monolayer of surfactant and therefore are well dispersed in the oil phase. In such well-dispersed aqueous phase, the dissolved metal cations can be hydrolyzed, precipitated, and/or reduced. The interface between the aqueous and oil phase is very important in the synthesis of nanoparticles, and it largely depends on the choice of surfactant and cosurfactant. For instance, Yang et al. [27] synthesized CdS quasi-nanospheres, nanoshuttles, nanowires, and nanotubes using water-in-oil microemulsion with different surfactants. It was shown that different surfactants provided different microemulsion templates that resulted in the formation of nanomaterials with unique morphologies and structures. Spirin et al. [28, 29] found that gold nanoparticles formed in Triton X-100 (TX-100)-based microemulsions were much smaller and more resistant to the oxidative degradations than those obtained in AOT-based microemulsions. The authors suggested that for nonionic surfactant, TX-100 gold nanoparticles were formed in the reverse micelle shell rather than in the micelle water pool.

In an earlier work, the substoichiometric magnetite nanoparticles were synthesized through the γ-irradiation of TX-100-based microemulsions [23, 24]. In this work, the water/Triton X-100/1-pentanol/cyclohexane microemulsions were used for the synthesis of gold nanoparticles. We have focused on the varying reducing conditions in the microemulsion and found that the size of gold nanoparticles, their aggregation, dispersion, and stability depend on the reducing conditions in microemulsions. More importantly, we found that AuNPs could be synthesized under highly oxidizing conditions, which motivated us to propose the base-catalyzed oxidation of alcohols (without using microemulsions) as a new synthesis route for obtaining gold nanoparticles.

Material and methods

Chemicals

Triton X-100 (polyoxyethylene(9) 4-(1,1,3,3-tetramethylbutyl)phenyl ether) and sodium borhydride ($NaBH_4$) p.a. were supplied by *Merck*. Gold (III) chloride trihydrate ($HAuCl_4 \cdot 3H_2O$), ≥99.9 % trace metals basis, was supplied by *Sigma Aldrich*. Cyclohexane, acetone, absolute ethanol, and amyl alcohol (1-pentanol) were of analytical purity, supplied by *Kemika* (Zagreb). Milli-Q deionized water with a resistivity 18 MΩ cm at 25 °C was used. $HAuCl_4$ 3.45 wt% stock solution was prepared by dissolving 1 g of $HAuCl_4 \cdot 3H_2O$ in 25 ml Mili-Q water.

Synthesis and characterization of samples

The chemical composition of pure microemulsions was obtained following the procedure by Yang et al. [27] and Gotić et al. [23, 24]. The two-microemulsion method was used. As the first step, microemulsion A and microemulsion B were prepared separately under the procedure shown in Scheme S1 in supplementary material. The water-to-surfactant-ratio (w_o) in both microemulsions

was 10 ($w_o = 10$). The water-in-oil microemulsion A contained 28 ml of cyclohexane (oil phase), 3 ml of Triton X-100 (surfactant), 1 ml of 4 wt% aqueous solution of $HAuCl_4$ (aqueous phase containing gold precursor), and 1 ml of 1-pentanol (co-surfactant). The water-in-oil microemulsion B had an identical chemical composition as microemulsion A with the difference that the composition of aqueous phase of microemulsion B was not the same. The chemical composition of aqueous phase of microemulsion B was adjusted from the highly reducing to the highly oxidizing requirements (Scheme S1). Then, the two microemulsions, one containing the gold precursor (microemulsion A) and the other reducing or oxidizing agent (microemulsion B), were mixed by adding microemulsion B to microemulsion A. The color of the thus-obtained microemulsion AB was pale yellow, reddish, or black depending on the synthesis conditions. Seven microemulsion samples were synthesized. The only parameter that was changed during the synthesis was the strength of reducing conditions in the microemulsions, which decreased from sample MAu-1 to MAu-7 (Scheme S1). The eighth sample was synthesized in a pure alcohol (1-pentanol) under oxidizing conditions. All syntheses were performed at room temperature.

Briefly, sample MAu-1 was synthesized (Scheme S1) in a way that aqueous phase of microemulsion B contained 1 ml of 0.4 M $NaBH_4$ dissolved in 0.4 M NaOH aqueous solution (high reducing condition). Samples MAu-2 to MAu-5 were synthesized in a way that aqueous phase of microemulsion B contained 1 ml of H_2O, whereas the reducing strength in microemulsions was controlled using γ-irradiation. The additional control of reducing strength was achieved by purging microemulsion with nitrogen gas prior the γ-irradiation (samples MAu-2 and MAu-3) or by γ-irradiation in the presence of dissolved oxygen (air) (samples MAu-4 and MAu-5). Samples MAu-4 and MAu-5 were synthesized using γ-irradiation at acidic (pH < 7) and alkaline (pH > 7) conditions, respectively. Samples MAu-6 (no particles) and MAu-7 were synthesized in a way that aqueous phase of microemulsion B contained 1 ml of H_2O (pH < 7) or 1 ml NaOH aqueous solution (pH > 7). The eighth sample Au-8 was synthesized (without microemulsion) by stirring 500 μl of 4 wt% aqueous solution of $HAuCl_4$, with 30 ml of 1-pentanol and with addition of 1 ml 0.4 M NaOH aqueous solution (pH > 7).

Synthesized samples were characterized as microemulsions or in some cases as solid samples. In order to obtain solid samples, the microemulsions were destabilized by adding acetone and the precipitates were isolated by centrifugation combined with successive washing in acetone and absolute ethanol. Isolated precipitates were dried under vacuum at room temperature and then characterized. Scanspeed 2236R High-speed centrifuge was used.

γ-irradiation was performed using a ^{60}Co source located in the Laboratory for Radiation Chemistry and Dosimetry, Division of Materials Chemistry at the Ruđer Bošković Institute. The dose rate of γ-radiation was ~8 kGy h^{-1}. The absorbed dose was 30 kGy per sample.

X-ray powder diffraction (XRD) patterns were recorded at 20 °C using APD 2000 X-ray powder diffractometer (CuKα radiation, graphite monochromator, NaI-Tl detector) manufactured by ITALSTRUCTURES, Riva Del Garda, Italy. The size and shape of AuNPs were evaluated using a probe Cs corrected Scanning Transmission Electron Microscope (STEM), model ARM 200 CF, and the thermal field emission scanning electron microscope (FE SEM, model JSM-7000 F) manufactured by *JEOL Ltd*. FE SEM was linked to the EDS/INCA 350 (energy-dispersive X-ray analyzer) manufactured by *Oxford Instruments Ltd.* The UV-Vis spectra of gold samples were recorded using a UV/VIS/NIR spectrometer Shimadzu model UV-3600. The quartz cells having 1-cm optical path length were used.

Results

Figure 1 shows the X-ray powder diffraction (XRD) patterns of samples MAu-1 and MAu-3. The XRD patterns of both samples fully coincide with the diffraction peaks of gold according to the ICDD (International Centre for Diffraction Data) card No.04-0784, indicating that both samples consist of gold (Au^0). The *hkl* Miller's indices of gold are given. By applying the Scherrer formula to the full width of the 111 line at half-maximum, the crystallite size of $D_{111} = 11.7$ and $D_{111} = 38.1$ nm can be estimated for samples MAu-1 and MAu-3, respectively. The calculated average crystallite size of the XRD lines 200 and 220 takes on lower values, which indicates slightly elongated gold crystals in both samples. In addition to that, sample MAu-3 possesses a very broad XRD maximum 2θ value of 20.0°. It was noted that in contact with a spatula, gelatinous powder black sample MAu-3 became liquid and then after some time solidified again (thixotropic sample). It can be assumed that the thixotropic properties of this γ-irradiated sample are due to the specifically arranged organic molecules and gold nanoparticles. Therefore, the broad XRD maximum 2θ value of 20.0° can be assigned to such poorly crystallized organic phase [8].

Figure 2 shows the TEM image of sample MAu-1 (a). The recorded sample MAu-1 was first isolated by centrifugation and then redispersed in ethanol. The inset shows particle size distribution in sample MAu-1. The discrete particles at the periphery of aggregates were considered for the calculation of the mean particle size ($\overline{D} = 7.2$) and standard deviation ($\sigma = 2.2$) using the normal function. The high-resolution TEM micrograph of sample MAu-1 is shown in panel (b). The arrow indicates the thickness of the organic layer which is

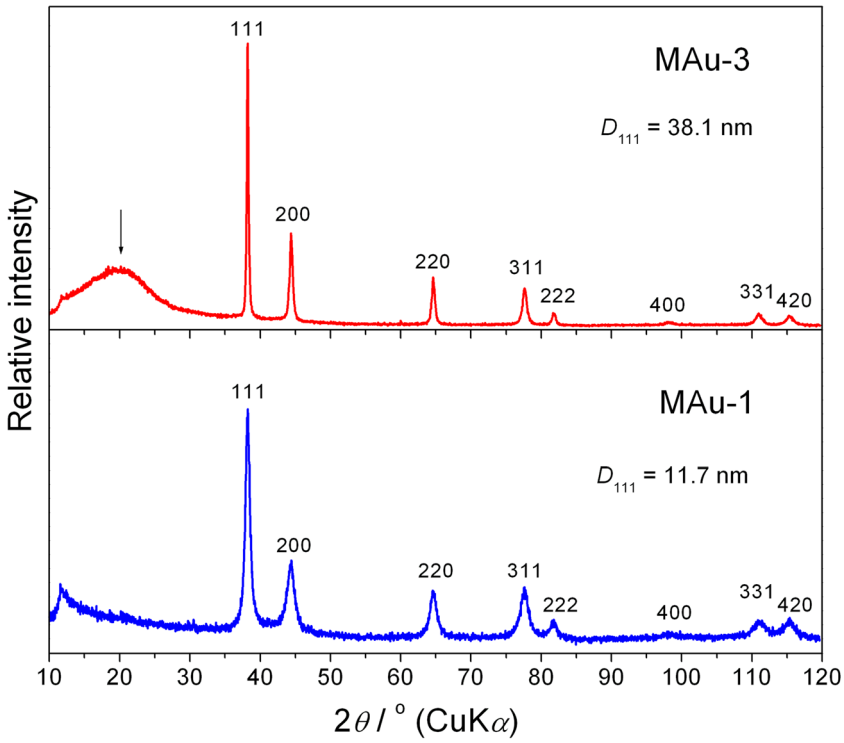

Fig. 1 X-ray diffraction patterns of samples MAu-1 and MAu-3. The Miller indices (*hkl*) are based on the ICDD card No. 04-0784. The calculated average crystallite sizes of the XRD lines 111 on the basis of line broadening (D_{111}) are 11.7 and 38.1 nm for samples MAu-1 and MAu-3, respectively. The very broad maximum 2θ value of 20.0° marked with an arrow in sample MAu-3 can be assigned to the poorly crystallized organic phase

0.94 nm at the point of the arrow. The equidistant planes of gold nanocrystals are well visible, which proves the high crystallinity of the sample. Some of the particles were twinned (as labeled particles with fivefold cyclic twins)

Figure 3 shows the SEM images of samples MAu-2 (a) and MAu-3 (b). The samples were synthesized under identical experimental conditions; the only difference was the initial concentration of the gold precursor which was twice higher in sample MAu-3 than in sample MAu-2. The samples were isolated by centrifugation and recorded as powders on a carbon support. Small nanoparticles approximately 15 nm in size and much larger coarse particles about 150 nm in size are visible in sample MAu-2 (a). The calculated particle size distributions are given in supplementary material.

Figure 4 shows the TEM micrograph of the mother liquor of the upper layer of sample MAu-4 (a). Discrete and well-dispersed nanoparticles 10 to 40 nm in size are visible. The inset shows calculated particle size distributions ($\overline{D}$ = 15.9 nm and σ = 4.4). The high-resolution TEM micrograph of the same sample (b) displays the particle shape of a triangle with rounded edges. Equidistant planes are clearly visible. The equilateral triangle particle is oriented in the [111] direction and most likely corresponds to the cross section obtained by cutting a cube particle centered at the origin with 111 planes.

Figure 5 shows the TEM micrographs of sample MAu-7. Discrete and well-dispersed nanoparticles are visible (a). The inset shows calculated particle size distributions ($\overline{D}$ = 11.9 nm and σ = 4.6). The high-resolution TEM micrographs of sample MAu-7 display pseudo-spherical particles approximately 10 nm in size (b) and particles that are in contact with each other (c).

Figure 6 shows the UV-Vis spectra of samples MAu-4 (a) and MAu-5 (b), immediately (0 h), 2.5 h, and 5 days following the γ-irradiation of microemulsions. These two samples were synthesized in the presence of dissolved oxygen using γ-irradiation. Sample MAu-4 was synthesized under acidic (pH <7), whereas MAu-5 was synthesized under alkali (pH > 7) conditions.

Figure 7 shows the UV-Vis spectra of sample MAu-7 taken at different times from the onset of synthesis. The UV-Vis spectrum of sample MAu-7 is characterized by a low UV-Vis maximum at 547 nm after 2 h, which shifts to 536 nm after 4 h and virtually does not change up to 100 h following the onset of synthesis. The absorbance reaches its maximum after 48 h and then begins to drop, thus indicating AuNP deposition at the bottom of the dish.

Figure 8 shows the SEM image (a) and corresponding particle size distribution (inset) of sample Au-8 synthesized using the base-catalyzed oxidation of 1-pentanol in alkaline media. The EDS is shown in panel (b). The insets show the photo of sample MAu-8 and the corresponding elemental analysis.

Figure 9 shows the XRD patterns of sample Au-8 synthesized using the base-catalyzed oxidation of 1-pentanol in alkaline media. The *hkl* Miller's indices of gold are given (ICDD card No. 04-0784). By applying the Scherrer formula to the full width of the 111 line at half maximum, the crystallite size of 11.7 nm can be estimated for this sample. The sharp

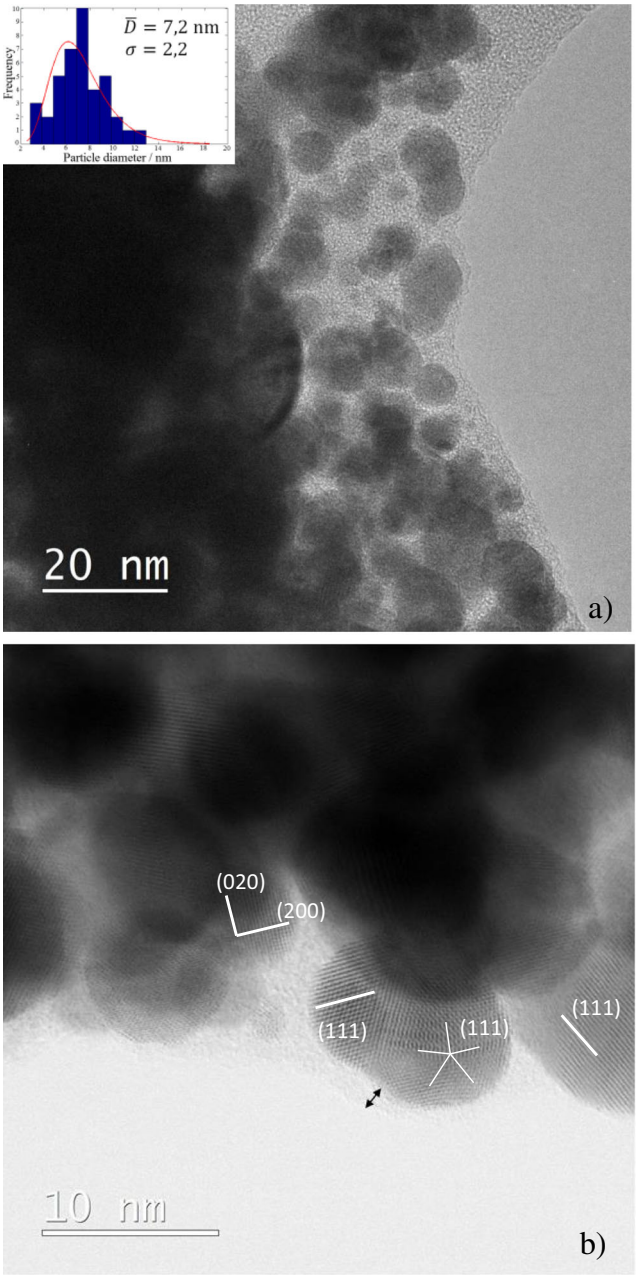

Fig. 2 TEM image of sample MAu-1 (**a**). The recorded sample MAu-1 was first isolated by centrifugation and then redispersed in ethanol. The *inset* shows particle size distribution of sample MAu-1. The mean particle size ($\overline{D}$ = 7.2) and standard deviation (σ = 2.2) were calculated using the normal function. The high-resolution TEM micrograph of sample MAu-1 is shown in (**b**). The *arrow* indicates the thickness of the organic layer which is 0.94 nm at the point of the arrow. Equidistant planes of gold nanocrystals are visible. Some of the particles were twinned (as labeled particles with a fivefold cyclic twin)

diffraction maxima symbolized with a number sign correspond to a small amount of NaCl because the sample was not washed in ethanol upon centrifugation. The diffraction maxima of very low intensity denoted with an asterisk correspond to an unidentified phase.

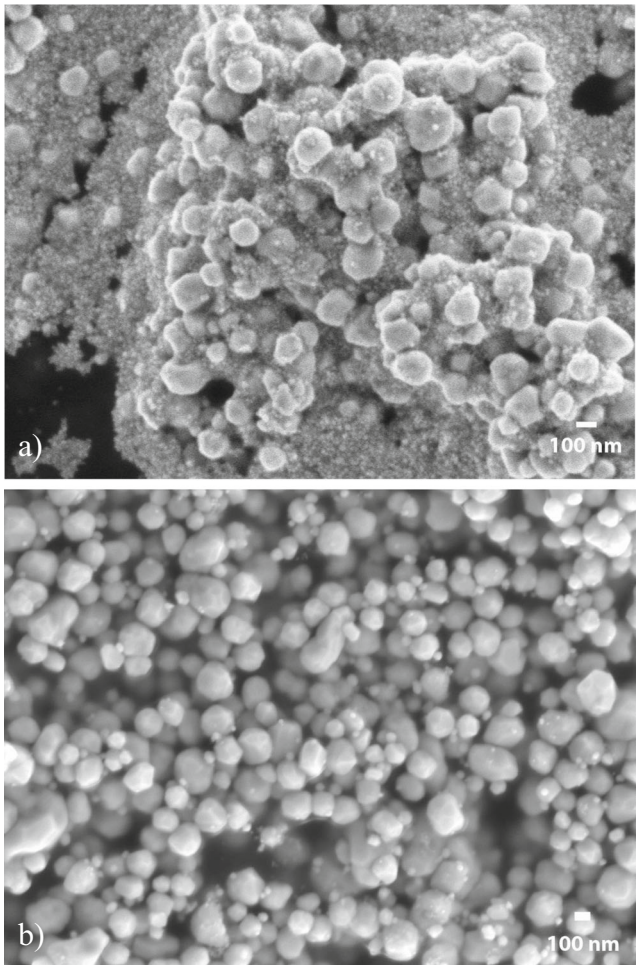

Fig. 3 SEM images of samples MAu-2 (**a**) and MAu-3 (**b**) synthesized under identical experimental conditions; the only difference was the initial concentration of the gold precursor that was twice higher in sample MAu-3 than in sample MAu-2. The samples were isolated by centrifugation and recorded as powders on a carbon support. Small nanoparticles approximately 15 nm in size and much larger coarse particles about 150 nm in size are visible in sample MAu-2 (**a**). Calculated particle size distributions are given in supplementary material (Fig. S2)

Discussion

Microemulsion synthesis of gold nanoparticles under very strong reducing conditions

The synthesis of colloidal gold, i.e., stable gold nanoparticles (AuNPs), in a medium involves two basic steps: (i) the reduction of gold ion Au(III) into elemental gold Au(0), and (ii) the stabilization of AuNPs in an aqueous or organic medium so that there is no change in particle size and/or the precipitation of gold nanoparticles. The $NaBH_4$ is a strong chemical reducing agent which reduced Au^{3+} ions into Au^0 according to this simplified chemical equation:

$$4\,Au^{3+} + 3\,BH_4^- + 9\,OH^- \rightarrow 4\,Au^0 + 3\,B(OH)_3 + 6\,H_2 \quad (1)$$

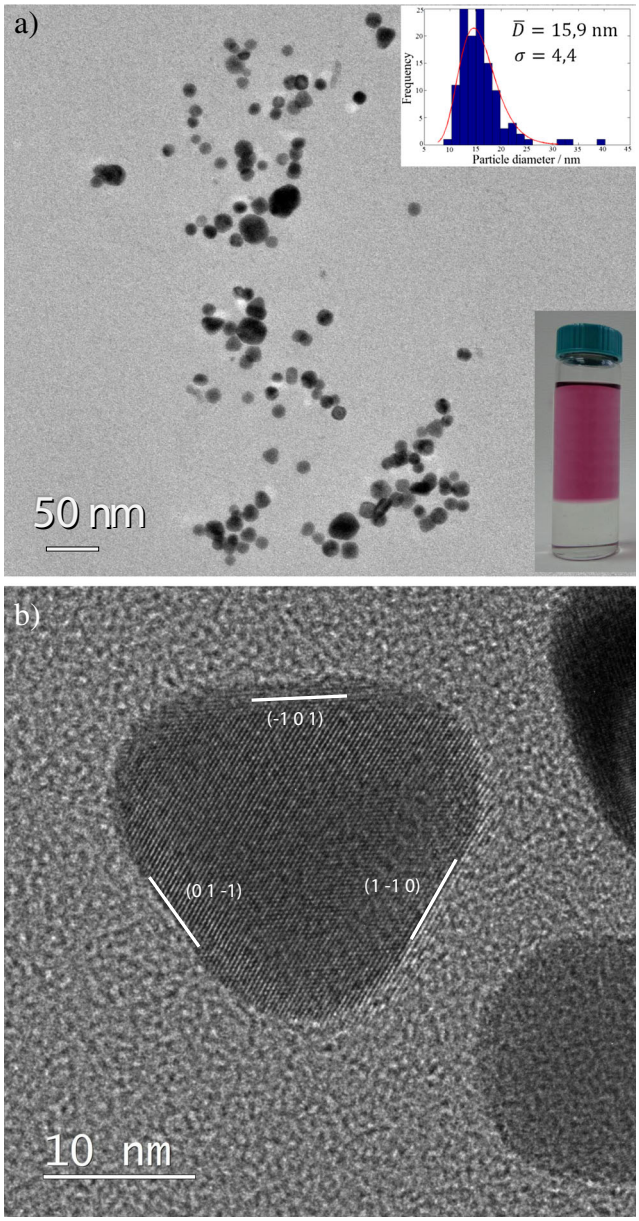

Fig. 4 TEM micrographs of the mother liquor of the upper layer of sample MAu-4 (**a**). Discrete and well-dispersed nanoparticles 10 to 40 nm in size are visible. The *inset* shows calculated particle size distributions. The calculated mean particle size using the normal function is $\overline{D}$ = 15.9 nm and σ = 4.4, where $\overline{D}$ and σ stand for the mean particle diameter and standard deviation, respectively. The high-resolution TEM micrograph of the same sample (**b**) displays the particle shape of a triangle with rounded edges. Equidistant planes are clearly visible. The equilateral triangle particle is oriented in the [111] direction and most likely corresponds to the cross section obtained by cutting a cube particle centered at the origin with 111 planes

According to literature sources [31], a rapid reduction of Au^{3+} ions with the strong reducing agent $NaBH_4$ in the aqueous phase as a rule leads to the formation of small gold nanoparticles (less than 10 nm). This can be explained by the rapid and complete reduction of Au^{3+} into Au^0 followed by the formation of a gold cluster, nucleation, and the growth of nuclei into nanometer gold particles. In this work, the crystallite size of 11.7 nm (XRD, Fig. 1) and the primary particle size of 7.2 nm (TEM, Fig. 2) were measured for sample MAu-1. However, the UV-Vis spectrum of sample MAu-1 possesses a characteristic surface plasmon resonance (SPR) band at 615 nm (supplementary Fig. S1), which suggests the presence of soft agglomerates in microemulsion. The position of the SPR band is regularly used for the determination of particle size. In this work, we have calculated particle size using the procedures presented by Haiss et al. [32] (for SPR ≤615 nm) and Khlebtsov [33] (for SPR > 615 nm). The size of AuNP aggregates in microemulsion determined using the Haiss model for the SPR band at 615 nm takes on a value of 148 nm (supplementary Table S1).

Sample MAu-1 was isolated by centrifugation and then dried in vacuum. The thus-obtained solid sample was hard and monolith (glass-like). Furthermore, it was very difficult to redisperse the sample in an aqueous or organic medium. Figure 2 shows the TEM image of redispersed sample MAu-1. The pronounced compactness of isolated sample MAu-1 and difficulties in its redispersion in aqueous media indicate that $NaBH_4$ had strong influence not only on the formation of gold nanoparticles but also on the polymerization of the organic phase in microemulsion. Moreover, the oxidation of $NaBH_4$ up to borate $(BO_3)^{3-}$ that readily polymerizes to a glass-like structure cannot be excluded.

Microemulsion synthesis of gold nanoparticles under moderately strong reducing/oxidizing conditions

The use of the strong chemical reducing agent $NaBH_4$ leads to a rapid reduction of gold ions in the microemulsion and the synthesis of gold nanoparticles. In this work, the moderately strong reducing or oxidizing conditions in microemulsions were achieved using γ-radiation. Moreover, the reducing/oxidizing properties of γ-irradiation were finely tuned by adjusting the atmosphere in the microemulsions. γ-radiation is an electromagnetic radiation of high energy (1.25 MeV). Microemulsion consists of an aqueous and an oil phase and of the water/oil interface; all phases can be ionized using γ-irradiation. The gold precursor ($HAuCl_4$) is dissolved in the aqueous phase which under γ-irradiation generates a variety of species [34–38]:

$$H_2O \rightsquigarrow e^-_{aq}, H_3O^+, H^\bullet, {}^\bullet OH, H_2, H_2O_2, H^+, HO_2^\bullet \quad (1)$$

The hydrated electron (e^-_{aq}) and hydrogen radical ($H^\bullet$) are strong reducing species, whereas the hydroxyl radicals ($^\bullet OH$) are very strong oxidizing species. When we want to ensure strong reducing conditions, the radical scavengers such as 2-propanol for scavenging hydroxyl radicals ($^\bullet OH$) should be used. In addition to that, the medium should be purged with

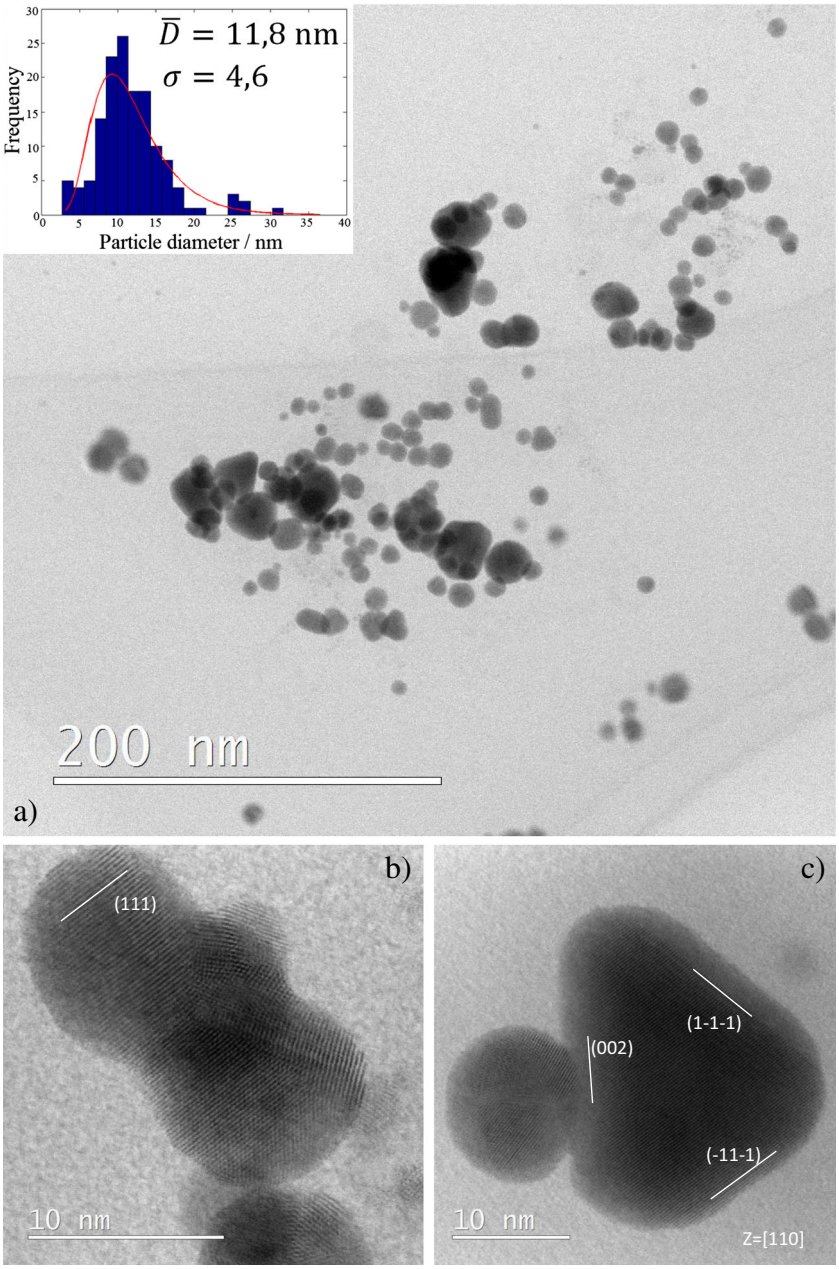

Fig. 5 TEM micrographs of sample MAu-7. Discrete and well-dispersed nanoparticles are visible (**a**). The *inset* shows calculated particle size distributions ($\overline{D}$ = 11.8 nm and σ = 4.6). The high-resolution TEM micrographs of sample MAu-7 display pseudo-spherical particles approximately 10 nm in size (**b**) and particles that are in contact with each other (**c**)

nitrogen prior to γ-irradiation in order to remove oxygen dissolved in media. The concentration of oxygen in a saturated aqueous solution at room temperature is about $1.3 \cdot 10^{-3}$ mol dm^{-3}. If the medium is not purged with nitrogen strong reducing agents, hydrated electron (e^-_{aq}) and hydrogen radical ($H^\bullet$) will react with oxygen according to the following equations:

$$e^-_{aq} + O_2 \rightarrow O_2^{\cdot -} \quad (3)$$

$$H^\cdot + O_2 \rightarrow HO_2^\cdot \quad (4)$$

The resulting superoxide $O_2^{\bullet -}$ and perhydroxyl $HO_2^\bullet$ radicals have oxidizing properties. Therefore, by bubbling the microemulsion with nitrogen (deoxygenated microemulsion), the reducing properties of γ-irradiation will be ensured, whereas the microemulsions that are not bubbled with nitrogen (air saturated microemulsions) will highlight the oxidizing properties of γ-irradiation. The mechanism of radiation-induced degradation of Triton X-100 in an oxygenated aqueous system was reported by Perkowski and Mayer [34].

In a previous work [21], it was shown that AuNPs could be synthesized by the citrate-radiolytical method using neither scavengers nor stabilizers. Besides, the citrate-radiolytical reduction took place in the presence of dissolved oxygen. In this work, samples MAu-2 and MAu-3 have been synthesized using γ-irradiation of deoxygenated microemulsions under acidic

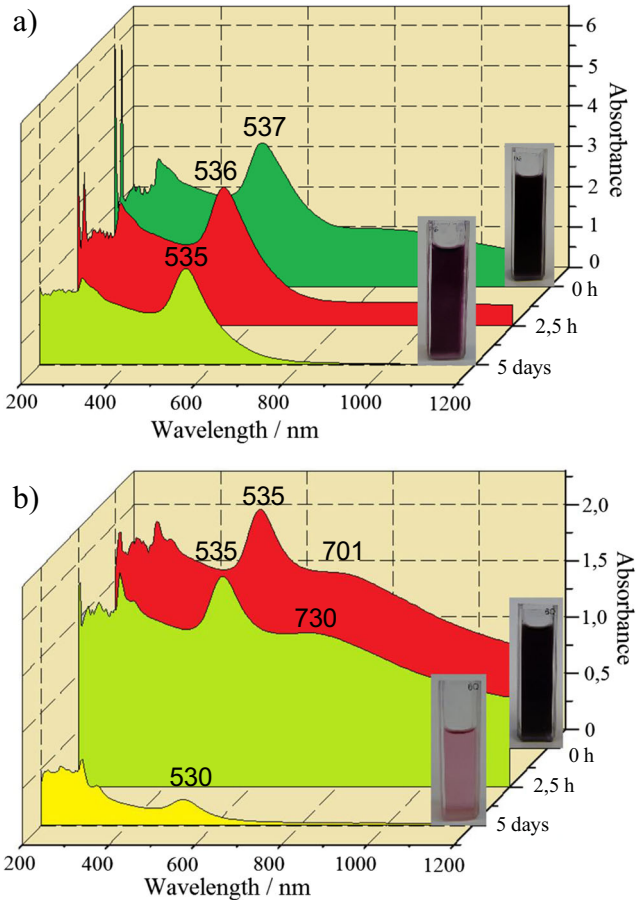

Fig. 6 UV-Vis spectra of microemulsions MAu-4 (**a**) and MAu-5 (**b**) following γ-irradiation; immediately (0 h) with corresponding photo (*red spectrum*), 2.5 h without the photo, and 5 days with corresponding photo (*yellow spectrum*). Sample MAu-4 was synthesized at pH < 7, whereas sample MAu-5 at pH > 7

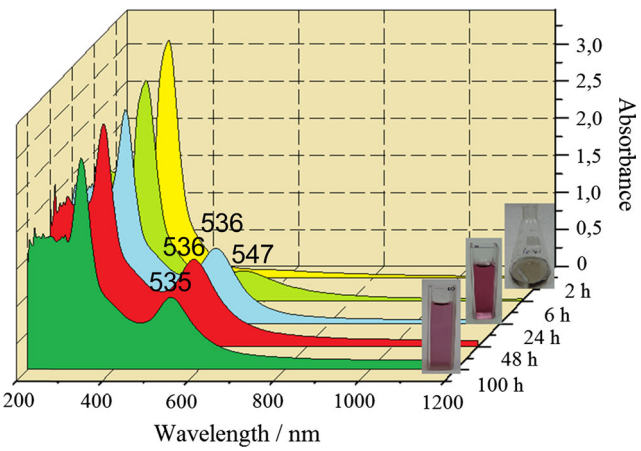

Fig. 7 UV-Vis spectra of sample MAu-7 taken at different times from the onset of synthesis; for the sample taken at 2 h (*yellow spectrum*), 6 h (light *blue spectrum*), and 100 h (*green spectrum*), the corresponding photos of samples are shown. The sample taken at 2 h (flask, *yellow spectrum*) is almost completely of yellow color, which is in accordance with very weak UV-Vis maximum at 547 nm

conditions (pH < 7). Both AuNP samples exhibited extraordinary properties; they are thixotropic and the AuNPs particle size alters significantly upon isolation by centrifugation. Besides, the concentrations of gold atoms in these samples are relatively high (AuNP preconcentration of gold; supplementary Fig. S2). The properties of samples MAu-2 and MAu-3 before and after centrifugation are described in the supplementary materials (supplementary Figs. S2, S3, S4, and S5).

The main question that arises is why the 15-nm-sized gold nanoparticles aggregated into large preconcentrated gold nanoparticles approximately 150 nm in size following the centrifugation of microemulsions. A possible explanation for this phenomenon is as follows: The solubility and dispersion of water-in-oil aggregates (reverse micelles) in the oil phase may be affected by the chemical composition of microemulsion and/or temperature. Above certain critical temperature (cloud point), the optically isotropic microemulsion becomes turbid and separates (delaminates) into two isotropic phases. One, a liquid phase will contain predominantly organic molecules with a large proportion of the surfactant (a surfactant-rich phase), and the other will comprise an aqueous-rich phase with a much smaller proportion of the surfactant (a surfactant-lean phase). In this way, the organic molecules that are related to the surface active agent will be extracted from an aqueous-rich phase and concentrated in a small volume of the surfactant-rich phase. Centrifugation promotes such separation of microemulsions into two phases, and the technique is referred to as the cloud point extraction [39–42]. With this cloud point (coacervate) technique, it is possible to extract and preconcentrate the gold present in trace amounts in natural aqueous samples to the small volume of organic micellar-rich phase and then analytically determine the exact concentration of gold in the samples [39, 40]. In the present case, the experimental results confirmed a significant change in the mean particle size of gold nanoparticles upon centrifugation (supplementary Fig. S3). The EDS analysis confirmed the preconcentration of gold in samples MAu-2 and MAu-3 (supplementary Fig. S3). All this suggested that these large preconcentrated gold nanoparticles were formed due to the cloud point extraction. It is reasonable to assume that the delaminated aqueous phase contained some quantity of Au(I)-organic complexes generated upon the γ-irradiation of microemulsion. Such Au(I) ions cannot be reduced into Au(0) in an aqueous phase; however, when these Au(I)-organic species are transferred to the organic-rich phase due to the cloud point extraction, a rapid increase in the aggregation number of the surfactant's micelles results in the precipitation of gold nanoparticles in a small volume of the organic-rich phase at the bottom of the tube. Due to these reasons, the concentration of precipitated large AuNPs is proportional to the initial concentration of gold in the microemulsion. Besides, the thus-obtained large AuNP preconcentration of gold (supplementary Fig. S3) and their particle size distributions are highly polydisperse (supplementary Fig. S2). One can

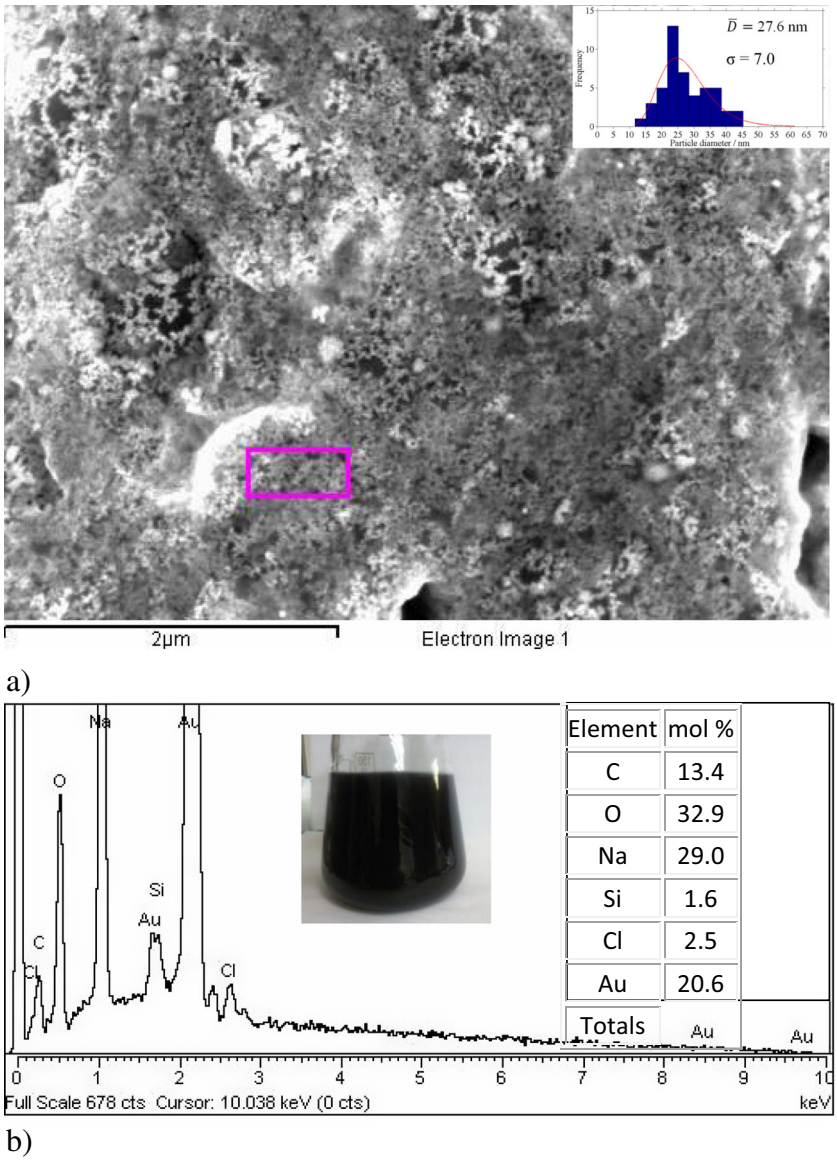

Fig. 8 SEM image (**a**) and the corresponding particle size distribution (*inset*) of sample Au-8 synthesized using the base-catalyzed oxidation of 1-pentanol in alkaline media. The EDS analysis results are given in (**b**). The *insets* show the photo of sample MAu-8 and the elemental analysis

argue that the cloud point of TX-100-based microemulsion cannot be reached at room temperature because Triton X-100 has a cloud point at 67 °C; however, alcohols and/or a small quantity of inorganic salt can lower the cloud point of TX-100-based microemulsions to a temperature below RT and centrifugation only favors such separation [39].

Following isolation by centrifugation, MAu-2 and MAu-3 samples exhibited thixotropic properties. Thixotropy was first observed in iron hydroxide by Schalek and Szegvár [43], whereas the term thixotropy was first used by Peterfi 1927 as a combination of the Greek words thixis (mixing or agitation) and trepo (tilting or changing) [44]. It was noted that in contact with a spatula, gelatinous powder samples MAu-2 and MAu-3 became liquids which after some time again spontaneously solidified. It can be assumed that the thixotropic properties of these samples are due to the specific structural organization of organic molecules with gold. It can be further assumed that a broad diffraction peak in sample MAu-3 at $2\theta = 20°$ (Fig. 1b) belongs to such poorly crystallized organic molecules [8]. Thixotropy is an important property of nanomaterials in view of their possible biomedical applications, for instance as injectable hydrogels [45].

The γ-irradiation of microemulsions in the presence of dissolved oxygen in the acidic range (sample MAu-4) resulted in suspended and relatively stable AuNPs (up to 5 days, Fig. 6a). At pH > 7 (sample MAu-5), AuNPs deposited much faster (Fig. 6b), which indicates the influence of pH on the stability of obtained gold nanoparticles. High backgrounds in the UV-Vis spectra of sample MAu-5 are very probably due to the formation of unstable organic molecules generated upon γ-

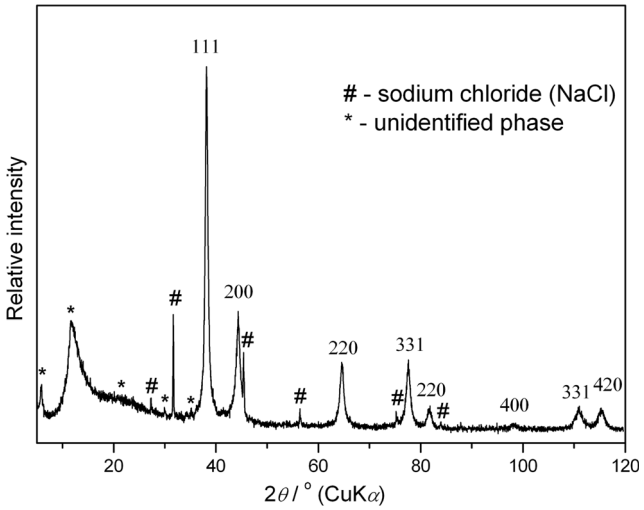

Fig. 9 XRD patterns of sample Au-8 synthesized using the base-catalyzed oxidation of 1-pentanol in alkaline media. The (*hkl*) Miller's indices of gold are given (ICDD card No. 04-0784). The crystallite size of 11.7 nm can be estimated for this sample on the basis of broadening the 111 line. The sharp diffraction maxima symbolized with the *number sign* correspond to a small amount of NaCl, since the sample was not washed in ethanol following the centrifugation. The diffraction maxima of very low intensities denoted with *asterisk* correspond to an unidentified phase

irradiation. These organic intermediates can be formed by the oxidation of an organic phase upon γ-irradiation at the pH > 7 [21]. In addition to that, small 1–2-nm gold nanoparticles which have no plasmonic maximum may contribute to the increase in the UV-Vis background [30].

The centrifugation of microemulsion MAu-4 produced two sharply separated layers (delaminated microemulsion) with well-dispersed and very stable gold nanoparticles sized 15.9 ±4 nm in the top layer (Fig. 4). It was suggested by Spirin et al. [29] that the top layer contained AuNPs stabilized by surfactant molecules and no water, whereas the underlayer consisted of disordered or locally ordered particles of water and organic molecules separated by the surfactant. Accordingly, the results presented in Fig. 4 show gold nanoparticles that are completely extracted from an aqueous-rich phase (underlayer) to an organic phase (top layer).

Microemulsion synthesis of gold nanoparticles under oxidizing conditions

The attempt to synthesize AuNPs in microemulsion without adding a reducing agent (oxidizing condition) in the acidic range (pH < 7) was not successful, as confirmed by the absence of the plasmonic maximum in the UV-Vis spectrum of sample MAu-6 (results not shown). Under higher oxidizing conditions in the alkaline range (NaOH aqueous solution, pH > 7), well-dispersed gold nanoparticles about 12 nm were formed (Sample MAu-7, Fig. 5). The AuNP concentrations in the microemulsion were gradually rising up to 48 h from the onset of the reaction (Fig. 7). Under the oxidizing conditions, relatively uniform and well-dispersed AuNPs slowly formed near the surfactant layer. The formation of AuNPs in microemulsion near the water-in-oil microemulsion shell can be explained by the oxidation of alcohol (hydroxyl, –C–OH) to carbonyl (>C=O) groups [29] aided by the catalytic action of hydroxide ions and gold [6, 9]. In parallel with the catalytic oxidation of alcohol groups in the microemulsion, gold ions were reduced, with a subsequent formation of gold nanoparticles. The microemulsion synthesis of gold nanoparticles in the alkaline range but not at an acidic pH refers to the catalytic action of hydroxide ions [6].

Synthesis of gold nanoparticles using base-catalyzed oxidation of alcohols at room temperature

Spirin et al. [28, 29] suggested that gold nanoparticles in a TX-100-based microemulsion were formed in the reverse micellar shell due to the oxidation of alcohol groups at the end of oxyethylene chains in the TX-100 surfactant. However, if the oxidation of the alcohol group is responsible for the reduction of Au(III) and a subsequent formation of gold nanoparticles, maybe it is not necessary that the alcohol groups be placed at the end of oxyethylene chains in TX-100. In this paper, 1-pentanol was used as a cosurfactant in microemulsion synthesis. To test whether the oxidation of 1-pentanol in the alkaline range can reduce Au(III) into Au(0), 500 μl of the 4 wt% $HAuCl_4$ solution and 1 ml of the 0.4 M NaOH aqueous solution were added to 30 ml of 1-pentanol and stirred at room temperature. The pH of such a solution was 10–11, and the molar ratio of Au(III)/NaOH/1-pentanol was the same as in the microemulsion sample MAu-7. In this experiment, a transparent solution in the induction period of about 5 to 10 min upon stirring began to darken and a black suspension was formed in the flask. A drop of the suspension was placed on the Si substrate, dried, and characterized using SEM. Figure 8 shows the SEM micrograph and a corresponding EDS analysis of the obtained black sample. The sample consisted of nanoparticles 27.6 ± 7 nm in size and contained around 20 mol % of gold. The EDS analysis (Fig. 8b) does not conclusively prove that the resulting particles corresponded to Au(0), because on top of gold (Au), the sample also contained a high amount of oxygen (O). Since there is a possibility that the analyzed nanoparticles are actually AuO and/or Au_2O_3, we perfomed an XRD analysis (Fig. 9). The XRD patterns demonstrate that the nanoparticles shown in Fig. 8 consist of gold, Au(0), as the dominant phase. The average crystallite size of gold calculated using the Sherrer method was estimated at 11.7 nm. Narrow XRD maxima (Fig. 9) belong to sodium chloride (NaCl) which was formed by neutralizing $HAuCl_4$ with added NaOH. The sample was not flushed with ethanol, so it consists of a small amount of NaCl crystals. The results of electron microscopy (Fig. 8) and the XRD analysis (Fig. 9) unambiguously indicate that the oxidation of alcohols

(1-pentanol) in the alkaline range can reduce Au(III) into Au(0) and form gold nanoparticles. 1-Pentanol cannot fully stabilize the resulting gold nanoparticles, and AuNPs slowly deposited on the bottom of the Erlenmeyer flask. The same experiment with 1-pentanol under acidic conditions did not produce gold nanoparticles, and the alcohol solution remained yellow, similar to the case of sample MAu-6. Hence, additional experiments involving 1-pentanol confirmed that the oxidation of alcohol was responsible for the formation of AuNPs in the alkaline aqueous-alcoholic medium (without the presence of a surfactant). The induction period before the appearance of the gold precipitate suggests that the reduction of Au(III) into Au(0) went through Au(I) since Au(0) could not have been formed until Au(III) was totally consumed [37, 38]. Besides, Au(I) ions adsorbed on gold clusters are easily reduced in unfavorable conditions, because the redox potential of gold ions adsorbed on the same metal clusters is more positive than the one of free ions in a solution [21, 38]. The same mechanism of Au(III) reduction could be applied to sample MAu-7 where the induction period of 2 h was observed (Fig. 7 and supplementary Table S1).

A selective catalytic oxidation of alcohol on gold nanoparticles (or gold metal) is the subject of intensive research [5–9]. This field of research is important for the pharmaceutical and agrochemical industries. It is environmentally more acceptable than the classical chemical oxidation of alcohol based on the use of toxic inorganic compounds such as chromates or permanganates. The mechanism of alcohol oxidation over gold support shows the involvement of hydroxide ions and gold. According to Kwon et al. [6], the most important first step in the oxidation of alcohol in the alkaline range is the deprotonation of alcohol by free hydroxide ions and creation of an alkoxide intermediate according to the following equation:

$$R{-}CH_2{-}OH_\alpha \xrightarrow{HO^-,\ pH > 7} R{-}CH_2{-}O^- + H_\alpha{}^+ \quad (5)$$

where H_α is hydrogen in the alcohol group. The resulting alkoxide is highly reactive and very susceptible to oxidation and serves as a precursor for the formation of aldehydes [6]:

$$R{-}CH_2{-}O^- \rightarrow R{-}CHO + H^+ + 2e^- \quad (6)$$

The aldehydes (R-CHO) are not stable in the alkaline range and can be further oxidized. Hydroxide ions (HO^-) adsorbed on the surface of gold nanoparticles significantly lower the energy barrier for the elimination of alkyl hydrogen [9]; hence, in these reactions, gold exhibits catalytic properties. On the contrary, the most important first step, the initial deprotonation of alcohol, does not depend on the catalytic properties of gold; it is base-catalyzed [6]. The first base-catalyzed step by free hydroxide ions (Eq. 5) explains very well why gold nanoparticles in 1-pentanol or in microemulsion were formed at the alkaline pH but not at the acidic pH. The formation of gold nanoparticles by base catalysis in 1-pentanol shows that gold nanoparticles can be synthesized without the use of a reducing agent. Moreover, gold nanoparticles in 1-pentanol were obtained by the oxidation of organic molecules in the presence of dissolved oxygen and free hydroxide ions (alkaline NaOH aqueous solution), which represents highly oxidizing conditions. Nevertheless, this work shows that such oxidizing conditions are crucial for the synthesis of gold nanoparticles. By the oxidation of a lower alcohol, for example, in the ethanol, propanol, or butanol, it is also possible to synthesize gold nanoparticles (results not shown). Moreover, by the use of 1-pentanol or higher alcohols in combination with an aqueous phase, AuNPs can be synthesized as a thin layer in the water/immiscible alcohol interface (results not shown). In conclusion, the base-catalyzed oxidation of alcohols at room temperature (without using microemulsions) can be used as a new, simple, and versatile synthesis route for obtaining AuNPs.

Conclusions

- In this work, gold nanoparticles (AuNPs) have been synthesized in a water-in-oil (w/o) microemulsion water/Triton X-100/1-pentanol/cyclohexane. All syntheses were performed at room temperature. The molar water-to-surfactant-ratio, i.e., the size of water droplets in microemulsion, was kept constant, and the only parameter that was varying during the synthesis was the strength of reducing agents.
- The size of gold nanoparticles, their size distribution and aggregation, dispersion, and stability in microemulsions highly depend on the reducing or oxidizing conditions during the synthesis and not on the size of water droplets.
- The surfactant Triton X-100 is not able to fully stabilize AuNPs in microemulsion. The exception is delaminated microemulsion where all gold nanoparticles are extracted, stabilized, and well-dispersed (suspended) in a surfactant-rich phase (Fig. 4), which is in line with the work by Spirin et al. [28, 29].
- The γ-irradiation of nitrogen-saturated microemulsion at the acidic pH produced gold nanoparticles of about 15 nm in size, which upon the cloud point extraction aggregated into large preconcentrated gold nanoparticles of about 150 nm in size. These gold nanoparticles possess thixotropic properties.
- The cloud point extraction technique can be used for the synthesis of preconcentrated gold nanoparticles.
- γ-irradition produced AuNPs in air-saturated microemulsions under highly oxidizing conditions.
- The addition of a NaOH aqueous solution to the microemulsion (pH > 7) generated rather uniform and well-dispersed AuNPs of 12 nm in size. The synthesis of AuNPs in microemulsion under oxidizing conditions at the pH > 7 is explained by the oxidation of alcohol (–

OH) to carbonyl (>C=O) groups [29] aided by the catalytic action of hydroxide ions and gold [6, 9].

- The synthesis of gold nanoparticles in 1-pentanol by adding the NaOH aqueous solution (pH > 7) at room temperature and without using microemulsion confirmed that the base-catalyzed oxidation of alcohols was crucial for the formation of gold nanoparticles.
- Based on the findings in this study, we propose the base-catalyzed oxidation of alcohols at room temperature as a new, simple, and versatile synthesis route for obtaining gold nanoparticles.
- The results of this study suggest that the classical approach of using a reducing agent for the synthesis of AuNPs is not a determining factor, since a diametrically opposite approach to the synthesis of AuNPs can be used, namely, stimulating the oxidation of the functional organic groups in close proximity to gold ions [21].

Acknowledgments The financial support of the Centre of Excellence for Advanced Materials and Sensors, "Ruđer Bošković" Institute, Croatia, is gratefully acknowledged. Goran Dražić acknowledges the financial support of the Slovenian Research Agency (ARRS) through Program No. P2-0393 and Project J2-6754. We thank Mr. Igor Sajko for the technical assistance on γ-irradiation.

References

1. Pal A (1998) Photoinitiated gold sol generation in aqueous Triton X-100 and its analytical application for spectrophotometric determination of gold. Talanta 46:583–587. doi:10.1016/S0039-9140(97)00320-2
2. Kwon MJ, Lee J, Wark AW, Lee HJ (2012) Nanoparticle-enhanced surface plasmon resonance detection of proteins at attomolar concentrations: comparing different nanoparticle shapes and sizes. Anal Chem 84:1702–1707. doi:10.1021/ac202957h
3. Jiao PF, Zhou HY, Chen LX, Yan B (2011) Cancer-targeting multifunctionalized gold nanoparticles in imaging and therapy. Curr Med Chem 18:2086–2102. doi:10.2174/092986711795656199
4. Dykman L, Khlebtsov N (2012) Gold nanoparticles in biomedical applications: recent advances and perspectives. Chem Soc Rev 41: 2256–2282. doi:10.1039/C1CS15166E
5. Ide MS, Davis RJ (2014) The important role of hydroxyl on oxidation catalysis by gold nanoparticles. Acc Chem Res 47:825–833. doi:10.1021/ar4001907
6. Kwon Y, Lai SCS, Rodriguez P, Koper MTM (2011) Electrocatalytic oxidation of alcohols on gold in alkaline media: base or gold catalysis? J Am Chem Soc 133:6914–6917. doi:10.1021/ja200976j
7. Vinod CP, Wilson K, Lee AF (2011) Recent advances in the heterogeneously catalysed aerobic selective oxidation of alcohols. J Chem Technol Biotechnol 86:161–171. doi:10.1002/jctb.2504
8. Yuan Y, Yan N, Dyson PJ (2011) pH-sensitive gold nanoparticle catalysts for the aerobic oxidation of alcohols. Inorg Chem 50: 11069–11074. doi:10.1021/ic201608j
9. Zope BN, Hibbitts DD, Neurock M, Davis RJ (2010) Reactivity of the gold/water interface during selective oxidation catalysis. Science 330:74–78. doi:10.1126/science.1195055
10. Nguyen DT, Kim D-J, Kim K-S (2011) Controlled synthesis and biomolecular probe application of gold nanoparticles. Micron 42: 207–227. doi:10.1016/j.micron.2010.09.008
11. Chang C-C, Chen C-P, Lee C-H et al (2014) Colorimetric detection of human chorionic gonadotropin using catalytic gold nanoparticles and a peptide aptamer. Chem Commun (Camb) 50:14443–14446. doi:10.1039/c4cc06366j
12. Tiwari PM, Vig K, Dennis VA, Singh SR (2011) Functionalized gold nanoparticles and their biomedical applications. Nanomaterials 1:31–63. doi:10.3390/nano1010031
13. Hainfeld JF, Slatkin DN, Smilowitz HM (2004) The use of gold nanoparticles to enhance radiotherapy in mice. Phys Med Biol 49: N309–N315
14. Reuveni T, Motiei M, Romman Z et al (2011) Targeted gold nanoparticles enable molecular CT imaging of cancer: an in vivo study. Int J Nanomedicine 6:2859–2864. doi:10.2147/IJN.S25446
15. Hainfeld JF, Slatkin DN, Focella TM, Smilowitz HM (2006) Gold nanoparticles: a new X-ray contrast agent. Br J Radiol 79:248–253. doi:10.1259/bjr/13169882
16. Jain S, Coulter JA, Hounsell AR et al (2011) Cell-specific radiosensitization by gold nanoparticles at megavoltage radiation energies. Int J Radiat Oncol Biol Phys 79:531–539. doi:10.1016/j.ijrobp.2010.08.044
17. Butterworth KT, McMahon SJ, Currell FJ, Prise KM (2012) Physical basis and biological mechanisms of gold nanoparticle radiosensitization. Nanoscale 4:4830–4838. doi:10.1039/c2nr31227a
18. Zhao P, Li N, Astruc D (2013) State of the art in gold nanoparticle synthesis. Coord Chem Rev 257:638–665. doi:10.1016/j.ccr.2012.09.002
19. Turkevich J, Stevenson PC, Hillier J (1951) A study of the nucleation and growth processes in the synthesis of colloidal gold. Discuss Faraday Soc 11:55–75. doi:10.1039/DF9511100055
20. Frens G (1973) Controlled nucleation for the regulation of the particle size in monodisperse gold suspensions. Nature 241:20–22. doi:10.1038/10.1038/physci241020a0
21. Hanžić N, Jurkin T, Maksimović A, Gotić M (2015) The synthesis of gold nanoparticles by a citrate-radiolytical method. Radiat Phys Chem 106:77–82. doi:10.1016/j.radphyschem.2014.07.006
22. Zieliska-Jurek A, Reszczyska J, Grabowska E, Zalesk A (2012) Nanoparticles Preparation Using Microemulsion Systems. Microemulsions - An Introduction to Properties and Applications
23. Gotić M, Jurkin T, Musić S (2007) Factors that may influence the micro-emulsion synthesis of nanosize magnetite particles. Colloid Polym Sci 285:793–800. doi:10.1007/s00396-006-1624-2
24. Gotić M, Jurkin T, Musić S (2009) From iron(III) precursor to magnetite and vice versa. Mater Res Bull 44:2014–2021. doi:10.1016/j.materresbull.2009.06.002
25. Uskoković V, Drofenik M (2005) Synthesis of materials within reverse micelles. Surf Rev Lett 12:239–277. doi:10.1142/S0218625X05007001
26. Moulik SP, Paul BK (1998) Structure, dynamics and transport properties of microemulsions. Adv Colloid Interf Sci 78:99–195. doi:10.1016/S0001-8686(98)00063-3
27. Yang X-H, Wu Q-S, Li L et al (2005) Controlled synthesis of the semiconductor CdS quasi-nanospheres, nanoshuttles, nanowires and nanotubes by the reverse micelle systems with different surfactants. Colloids Surf A Physicochem Eng Asp 264:172–178. doi:10.1016/j.colsurfa.2005.05.059
28. Spirin MG, Brichkin SB, Razumov VF (2005) Synthesis and stabilization of gold nanoparticles in reverse micelles of Aerosol OT and Triton X-100. Colloid J 67:485–490. doi:10.1007/s10595-005-0122-4
29. Spirin MG, Brichkin SB, Razumov VF (2008) Studies on absorption spectra of uniform gold nanoparticles prepared in Triton X-100 reverse micelles. J Photochem Photobiol A Chem 196:174–179. doi:10.1016/j.jphotochem.2007.12.014

30. Vô KDN, Kowandy C, Dupont L, Coqueret X (2015) Evidence of chitosan-mediated reduction of Au(III) to Au(0) nanoparticles under electron beam by using $OH^{\cdot}$ and e−aq scavengers. Chem Commun 51:4017–4020. doi:10.1039/C4CC09346A
31. Polte J, Ahner TT, Delissen F et al (2010) Mechanism of gold nanoparticle formation in the classical citrate synthesis method derived from coupled in situ XANES and SAXS evaluation. J Am Chem Soc 132:1296–1301. doi:10.1021/ja906506j
32. Haiss W, Thanh NTK, Aveyard J, Fernig DG (2007) Determination of size and concentration of gold nanoparticles from UV−Vis spectra. Anal Chem 79:4215–4221. doi:10.1021/ac0702084
33. Khlebtsov NG (2008) Determination of size and concentration of gold nanoparticles from extinction spectra. Anal Chem 80:6620–6625. doi:10.1021/ac800834n
34. Perkowski J, Mayer J (1994) Oxygen effect in the radiolysis of Triton X-100 aqueous solution. J Radioanal Nucl Chem Lett 188:211–217. doi:10.1007/BF02164594
35. Gachard E, Remita H, Khatouri J et al (1998) Radiation-induced and chemical formation of gold clusters. New J Chem 22:1257–1265. doi:10.1039/A804445G
36. Von Sonntag, C., Formation of Reactive Free Radicals in an Aqueous Environment, in: Free-Radical-Induced DNA Damage and Its Repair, Springer, Berlin, Heidelberg, 2006, pp. 7–46. http://link.springer.com/chapter/10.1007/3-540-30592-0_2
37. Abidi W, Remita H (2010) Gold based nanoparticles generated by radiolytic and photolytic methods. Recent Patents Eng 4:170–188. doi:10.2174/187221210794578556
38. Dey GR, El Omar AK, Jacob JA et al (2011) Mechanism of trivalent gold reduction and reactivity of transient divalent and monovalent gold ions studied by gamma and pulse radiolysis. J Phys Chem A 115:383–391. doi:10.1021/jp1096597
39. Urucu OA, Gündüz ZY, Yetimoğlu EK (2013) Cloud point preconcentration of gold (III) and determination by flame atomic absorption spectrometry. Indian J Chem Technol 20:106–110. http://nopr.niscair.res.in/handle/123456789/16542
40. El-Naggar WS, Lasheen TA, Nouh E-SA, Ghonaim AK (2010) Cloud point extraction and preconcentration of gold in geological matrices prior to flame atomic absorption determination. Cent Eur J Chem 8:34–40. doi:10.2478/s11532-009-0093-0
41. Samaddar P, Sen K (2014) Cloud point extraction: a sustainable method of elemental preconcentration and speciation. J Ind Eng Chem 20:1209–1219. doi:10.1016/j.jiec.2013.10.033
42. Melnyk A, Namieśnik J, Wolska L (2015) Theory and recent applications of coacervate-based extraction techniques. TrAC Trends Anal Chem 71:282–292. doi:10.1016/j.trac.2015.03.013
43. Schalek E, Szegvari A (1923) Die langsame Koagulation konzentrierter Eisenoxydsole zu reversiblen Gallerten. Kolloid-Zeitschrift 33:326–334. doi:10.1007/BF01427565
44. Barnes HA (1997) Thixotropy—a review. J Non-Newtonian Fluid Mech 70:1–33. doi:10.1016/S0377-0257(97)00004-9
45. Schon E-M, Bachl J, Diaz Diaz D (2014) Thixotropic and injectable nature of supramolecular aqueous gels derived from N, N'-dibenzoyl-L-cystine and the effects of esterification. Nanosci Nanotechnol Asia 4:31–37. doi:10.2174/2210681204666140905222744

Electronic supplementary material

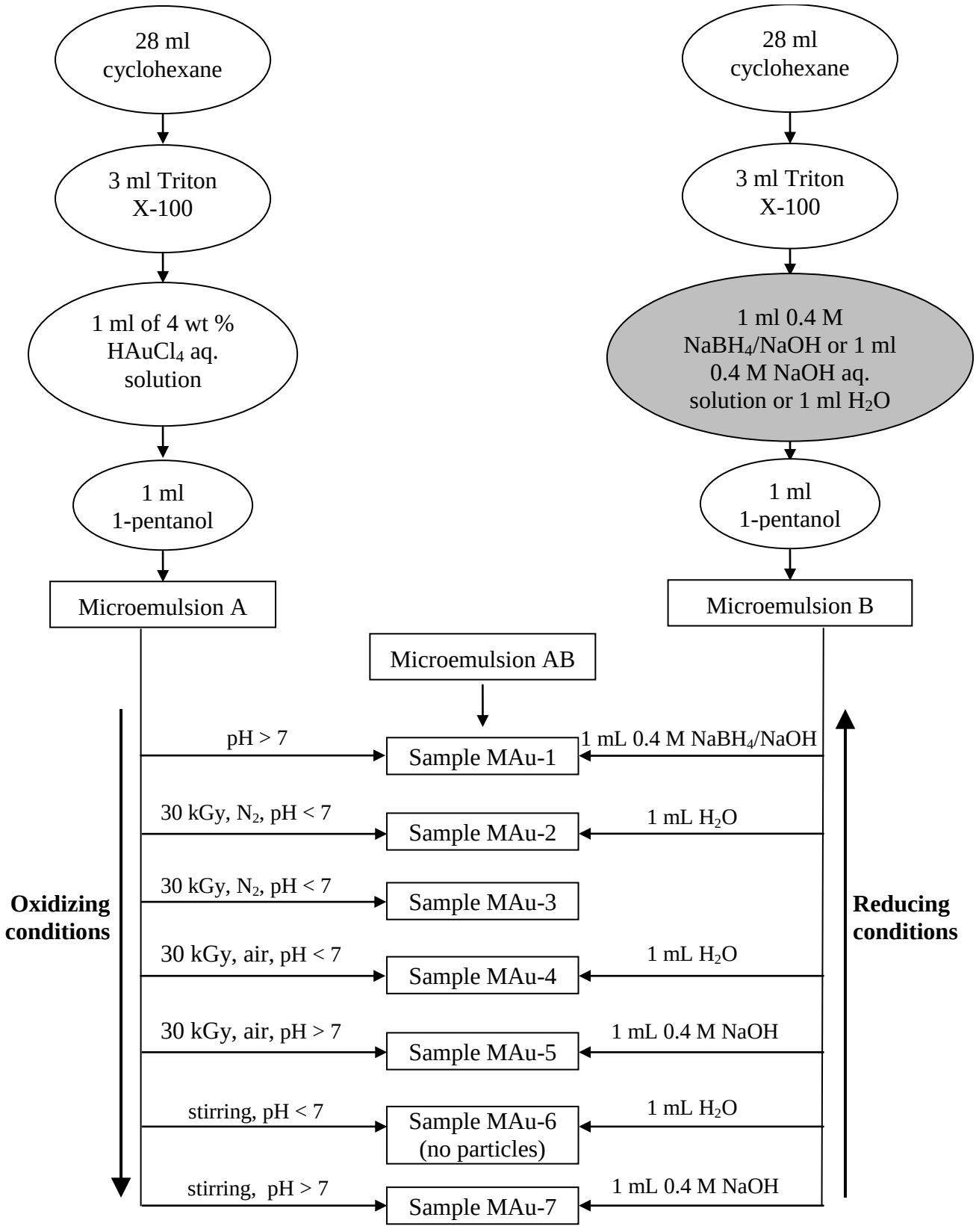

Additional experiments without microemulsion

500 μL 4 wt% $HAuCl_4$ + 30 mL 1-pentanol —(oxidation with NaOH aq. solution, pH > 7)→ Sample Au-8

Scheme S1

Table S1 UV-Vis, TEM and SEM characterization of samples. The gold nanoparticle size was determined from the UV-Vis spectra using a procedure presented by Haiss et al. [S1]. The method is based on the relative A_{SPR}/A_{450} ratio. For samples MAu-1 and MAu-3 the nanoparticle size was determined using a procedure presented by Khlebtsov [S2]. The mean particle size was calculated from TEM images using the normal function.

Sample	λ_{SPR} / nm	A_{SPR}	A_{450}	Gold particle size calculated from UV/Vis / nm	Mean gold particle size from TEM / nm	ε_{450} / $mol^{-1}\ dm^3\ cm^{-1}$	pH
MAu-1	615	3.63[a]		148	7.2 + aggregates	$2.03 \cdot 10^7$	8
MAu-2	538 690	2.33[a] 1.86[a]	1.70[a]	62 202	14.9[b] + 153.2[b]	$2.03 \cdot 10^7$	5
MAu-3	585	9.72[a]	4.50[a]	120	141.6[b]	-	-
MAu-4							
0 h	537 824	3.57 1.43	2.28	12 275	15.9[c]	$1.09 \cdot 10^8$	6
2.5 h	536	3.44	2.00	20		$2.67 \cdot 10^8$	
5th day	535	2.39	1.28	30		$1.96 \cdot 10^9$	
MAu-5							
0 h	536 701	2.13 1.57	1.58	6-7 202	-	$1.26 \cdot 10^7$	7.5
2.5h	535 730	1.88 1.37	1.40	6-7		$1.26 \cdot 10^7$	
5th day	530	0.23	0.15	11		$8.27 \cdot 10^7$	
MAu-6	no SPR band						6
MAu-7							
2 h	-						
6 h	547	0.40	0.33	4-5	11.9	$3.62 \cdot 10^6$	7.5
24 h	536	1.10	0.67	11		$8.27 \cdot 10^7$	
48 h	536	1.18	0.75	13		$1.39 \cdot 10^8$	
100 h	535	0.98	0.35	3-4		$1.49 \cdot 10^6$	
172 h	536	0.74					

[a] Obtained by multiplying the observed absorbance by its dilution factor (33.3% dilution).
[b] Determined from SEM images.
[c] Determined from TEM images of mother liquor of sample MAu-4.

References

S1. W. Haiss, N.T.K. Thanh, J. Aveyard, D.G. Fernig, Determination of Size and Concentration of Gold Nanoparticles from UV−Vis Spectra. Analytical Chemistry 79 (2007) 4215–4221

S2. N.G. Khlebtsov, Determination of Size and Concentration of Gold Nanoparticles from Extinction Spectra. Anal. Chem. 80 (2008) 6620–6625.

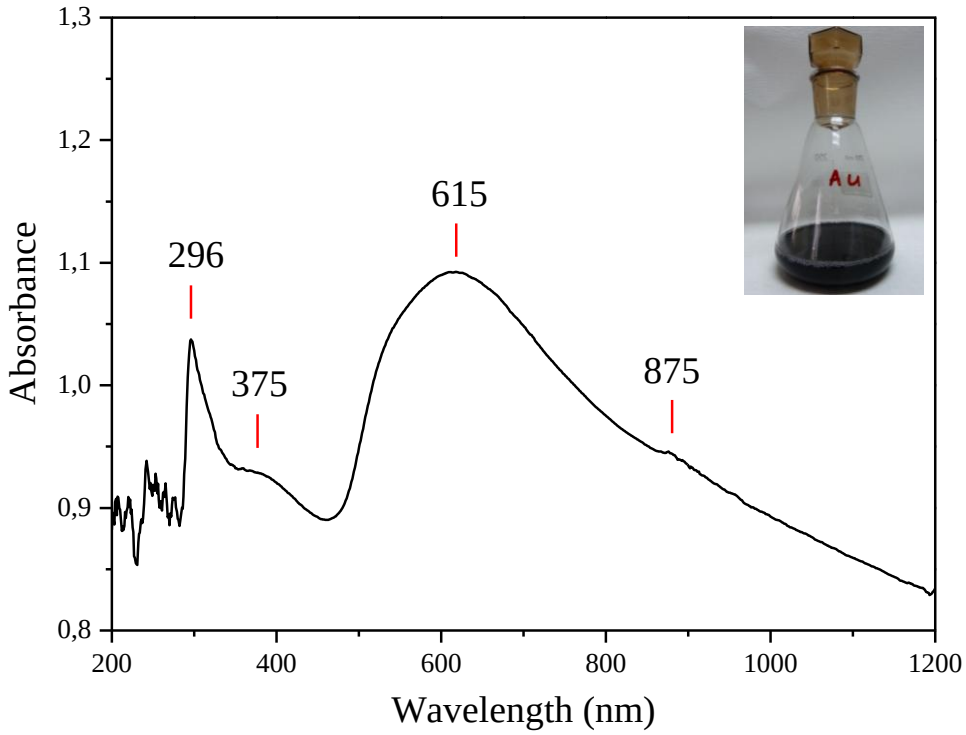

a)

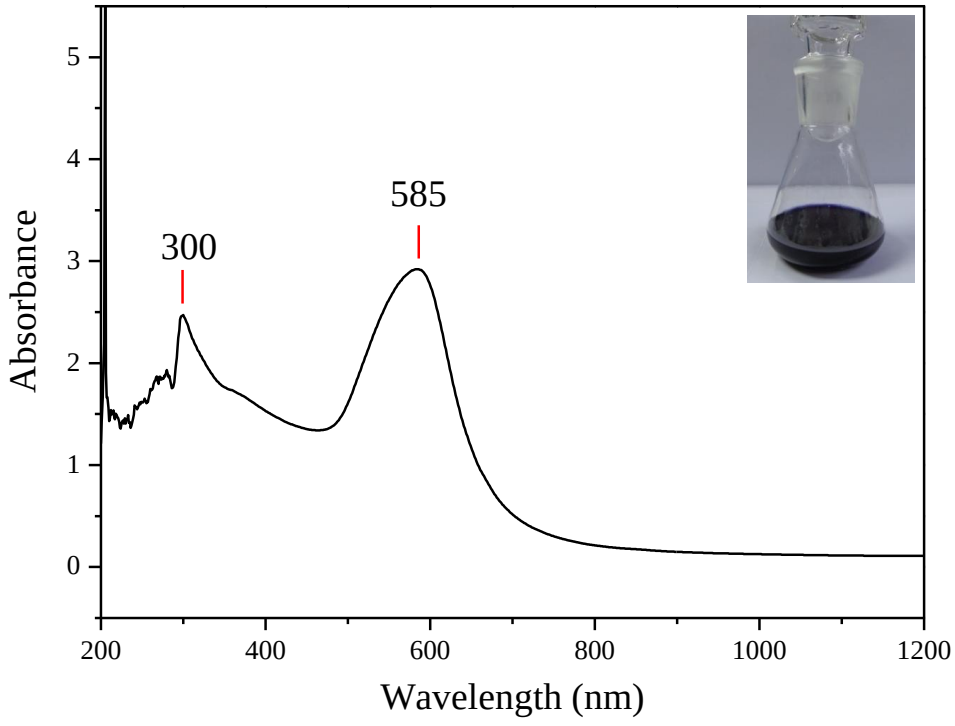

b)

Fig. S1 UV-Vis spectra of samples MAu-1 and MAu-3. Sample MAu-1 was diluted with „pure“ microemulsion at a ratio of 1 : 2 (33 % dilution), whereas sample MAu-3 was recorded as synthesized.

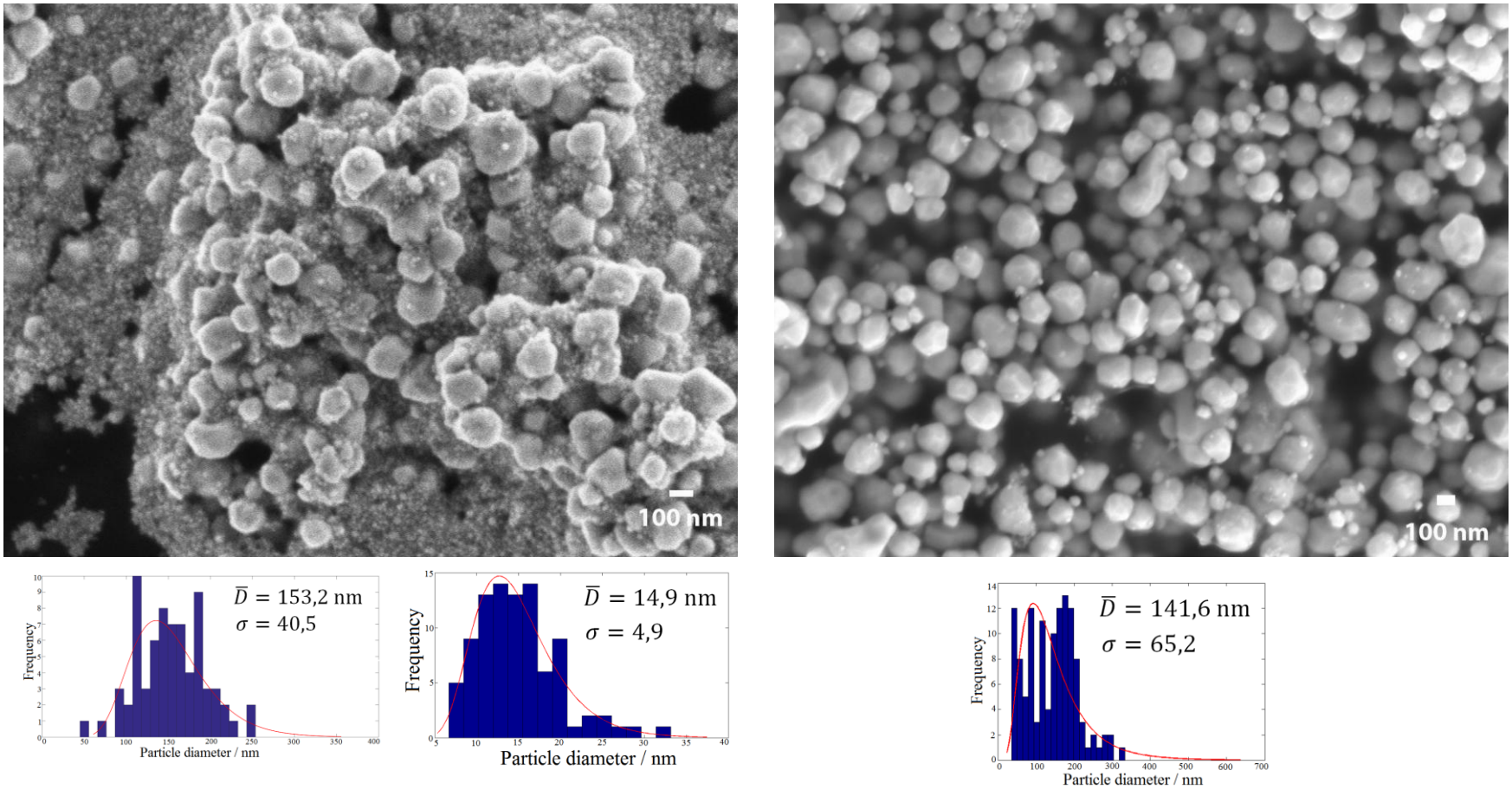

Fig. S2 SEM images of samples MAu-2 (A) and MAu-3 (B) isolated by centrifugation and recorded on a carbon support. Below the images are corresponding particle size distributions. For sample MAu-2 two size distributions are given, for small (14.9 nm) and large (153.2 nm) nanoparticles. The mean particle size was calculated using the normal function, where and σ stand for the mean particle diameter and standard deviation, respectively.

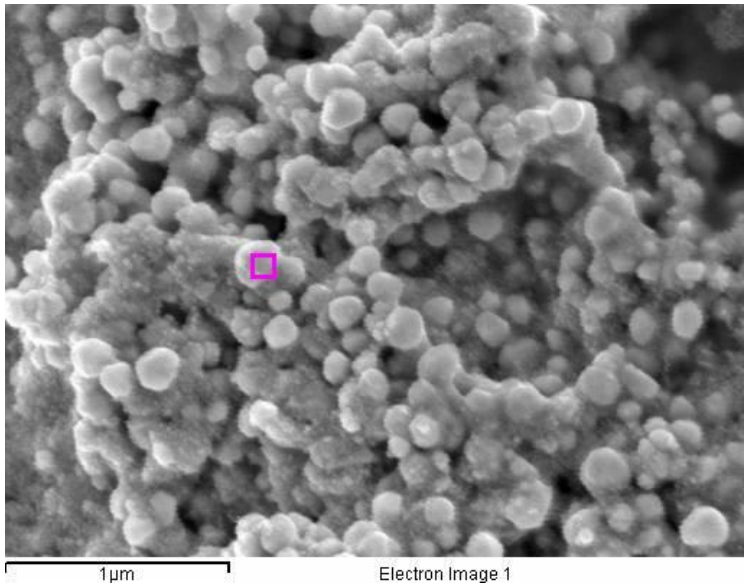

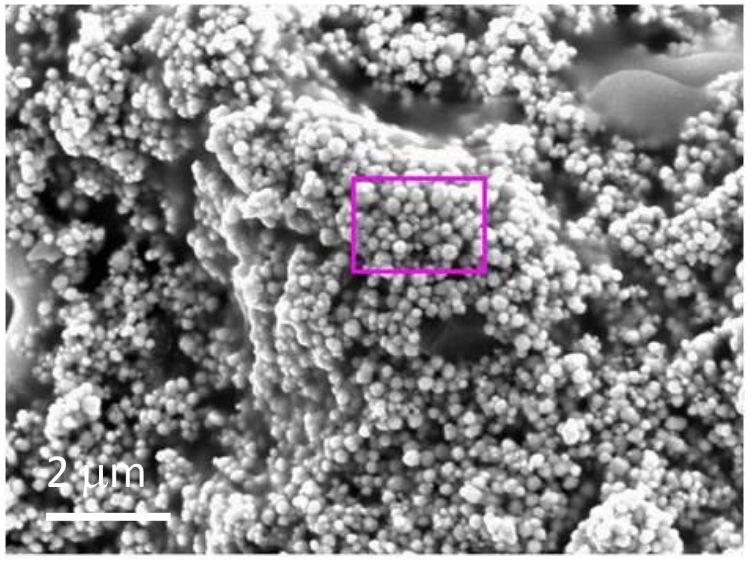

A) B)

Fig. S3 SEM images and corresponding EDS analyses of samples MAu-2 (A) and MAu-3 (B) upon centrifugation.

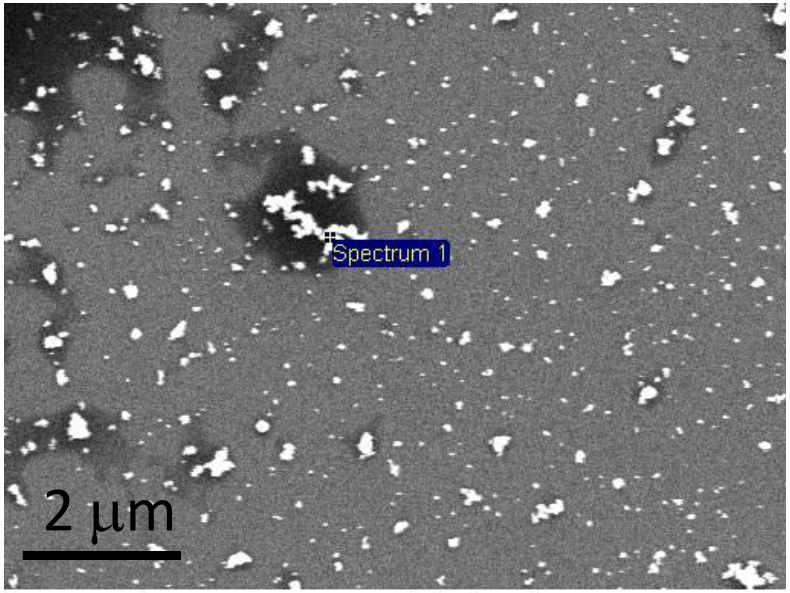

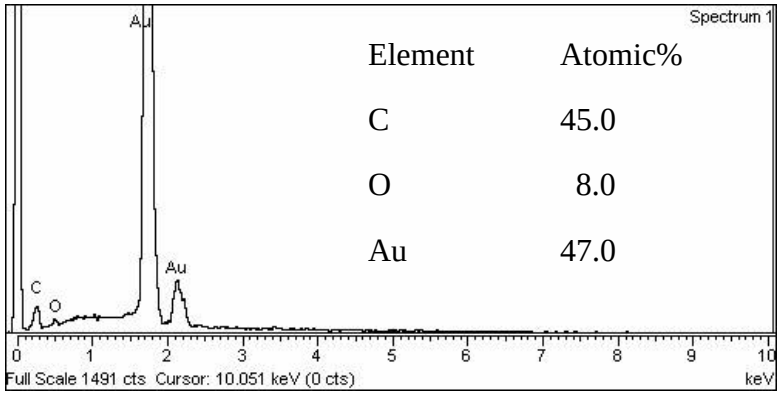

Element	Atomic%
C	45.0
O	8.0
Au	47.0

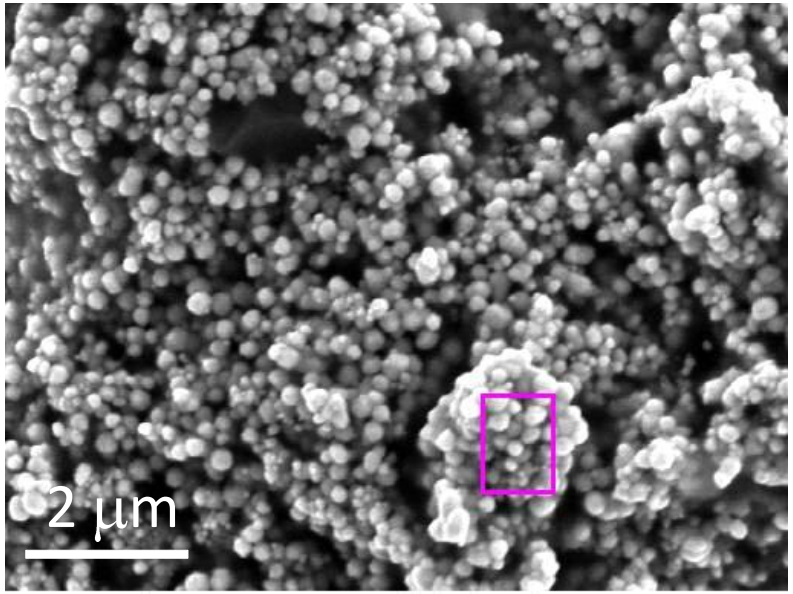

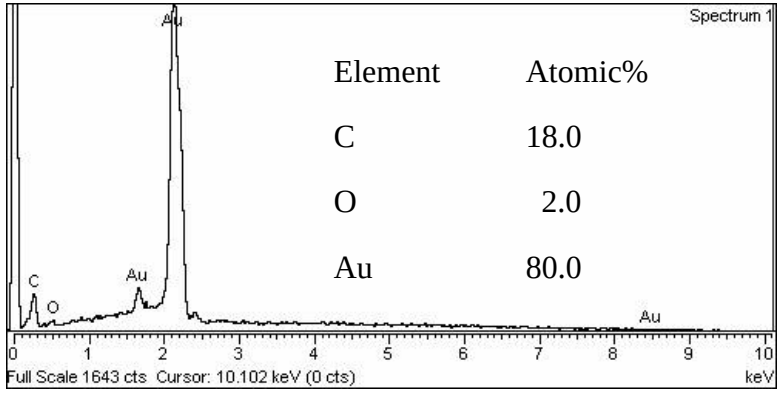

Element	Atomic%
C	18.0
O	2.0
Au	80.0

A) B)

Fig. S4 SEM images and corresponding EDS analyses of sample MAu-3 before (A) and after centrifugation (B). The relative concentration of gold rises and the size of nanoparticles increases upon centrifugation.

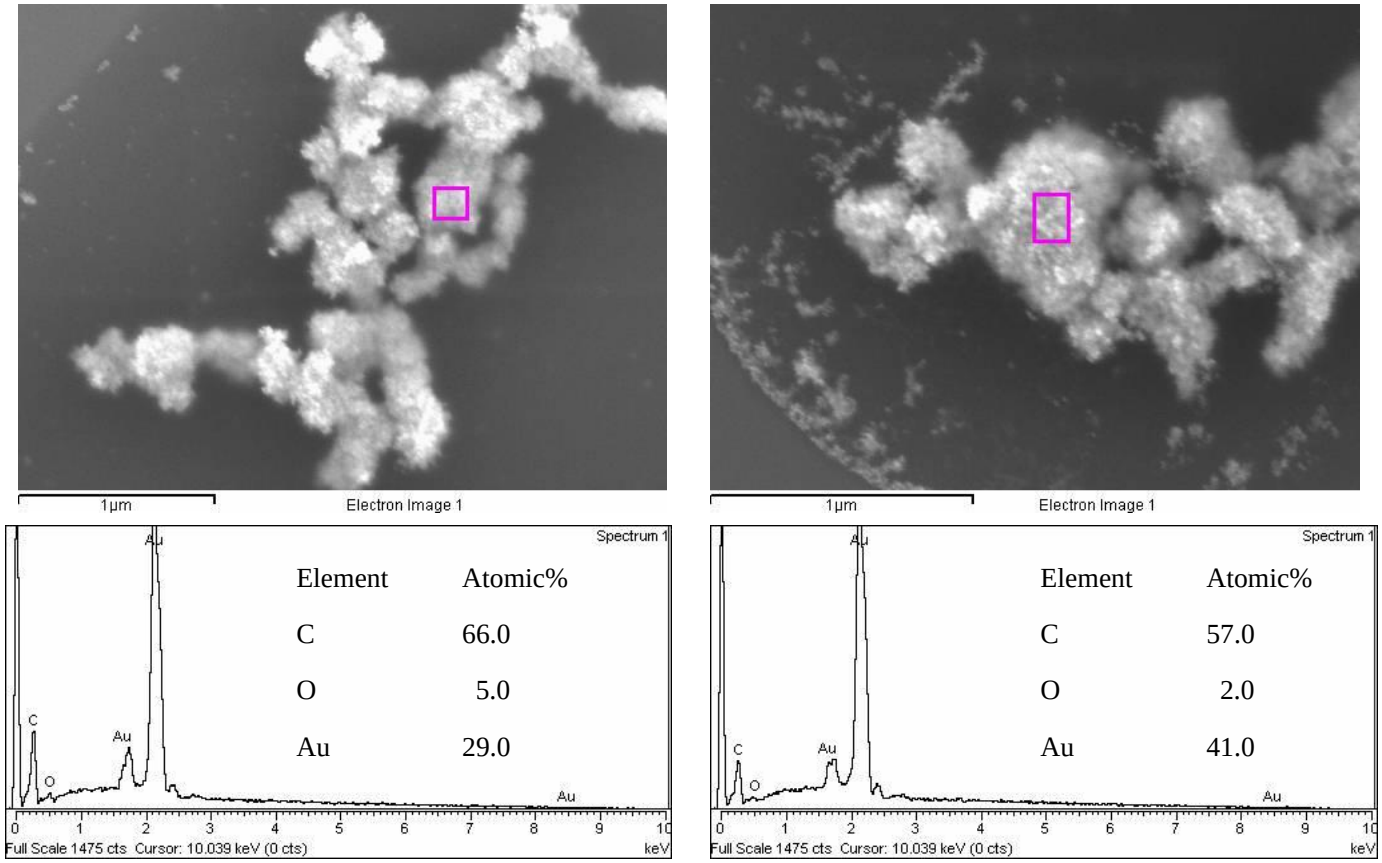

A) B)

Fig. S5 SEM images and corresponding EDS analyses of sample MAu-2 before (A) and after the addition of acetone (B). Both samples were analyzed as microemulsion (there was no centrifugation). The size of nanoparticles did not change before or after the addition of acetone. The relative concentration of gold was higher on addition of acetone, which suggests that the samples contained an amount of Au(I) ions that were reduced upon adding acetone. Generally, acetone is added to the microemulsion prior to centrifugation in order to impair its stability and facilitate the isolation of gold nanoparticles in the form of the precipitate (powder).